

INFLUENCE OF NOISE ON SUBWAVELENGTH IMAGING OF TWO CLOSE SCATTERERS USING TIME REVERSAL METHOD: THEORY AND EXPERIMENTS

M. Davy

Institut Langevin, ESPCI Paris Tech, CNRS UMR 7587
Laboratoire Ondes et Acoustique
Université Denis Diderot Paris
10 rue Vauquelin 75231 Paris cedex 05, France

J.-G. Minonzio

Laboratoire Imagerie Paramétrique
UMPC Université Paris 06, UMR 7623
15 Rue de l'École de médecine, 75006 Paris, France

J. de Rosny, C. Prada, and M. Fink

Institut Langevin, ESPCI Paris Tech, CNRS UMR 7587
Laboratoire Ondes et Acoustique
Université Denis Diderot Paris
10 rue Vauquelin 75231 Paris cedex 05, France

Abstract—Although classical imaging is limited by the Rayleigh criterion, it has been demonstrated that subwavelength imaging of two point-like scatterers can be achieved with probing sensors arrays, even if the scatterers are located in the far field of the sensors. However, the role of noise is crucial to determine the resolution limit. This paper proposes a quantitative study of the influence of noise on the subwavelength resolution obtained with the DORT-MUSIC method. The DORT method, French acronym for decomposition of the time reversal operator, consists in studying the invariants of the time reversal operator. The method is combined here with the estimator MUSIC (Multiple Signal Classification) to detect and image two close metallic wires. The microwaves measurements are performed between 2.6 GHz and 4 GHz. Two wires of $\lambda/100$ diameters separated by $\lambda/6$ are imaged and separated experimentally. To interpret this result in

terms of noise level, the analytical expression of the eigenvectors of the time reversal operator perturbed by the noise is established. We then deduce the noise level above which the subwavelength resolution fails. Numerical simulations and experimental results validate the theoretical developments.

1. INTRODUCTION

A dramatic issue for all detection and imaging techniques concerns the resolution. Here by resolution, we mean the capacity to separate two close point-like, or isotropic scatterers. Indeed, in the far field approximation, the diffraction limit is given by the Rayleigh criterion. If the array of probing sensors is used to focus the waves, the classical resolution is limited by $\lambda/2$, where λ is the wavelength of the illuminating field. However, some methods lead to overcome this limit in imaging. Multiple Signal Classification (MUSIC) is one of them. This method was investigated by Cheney [1]. Lev-Avri and Devaney combined first Time Reversal and MUSIC to achieve super-resolution [2]. This method is however very sensitive to the noise. Far field subwavelength resolution is consequently very challenging experimentally.

Without noise, unlimited resolution can be achieved. Nevertheless increasing the noise level degrades the quality of subwavelength imaging. Some papers underlined the sensitivity of the DORT-MUSIC method to the noise level, but, at our knowledge, no systematic study has been conducted. In particular no analytical expression of the resolution limit in presence of noise has been provided. The aim of this paper is thus to explore the influence of the noise level on the subwavelength imaging both experimentally and theoretically, using isotropic electromagnetic scatterers.

The DORT method has been developed in acoustics since 1994 [3]. It consists in studying the Time Reversal Invariants (TRI) of the Time Reversal Operator. This latter is built from the inter-element responses matrix between an emitting and a receiving array. The DORT method has been first applied to detect and focus selectively on different scatterers in a medium [3]. Till now it has been studied in different domains such as radar imaging [4], non-destructive evaluation [5, 6] or underwater acoustics [7]. The studies about the application of DORT method with microwaves began in 1999 with the work of Tortel et al.. They investigated the role of different polarizations for dielectric scatterers [8]. They showed experimentally that the DORT method leads to localize dielectric cylinders with a high precision and a low sensitivity to noise.

In 1996, Prada et al. performed the first study of the time reversal invariants to separate scatterers echoes and focus selectively on each of them [9]. Regarding subwavelength imaging, in 2003 Prada et al. showed that the DORT method leads to detect two wires distant from less than half a wavelength [10]. At best, they experimentally resolved $\lambda/3$ distant wires. To achieve such sub-wavelength resolution, they suggested combining the DORT method with two different non-linear signal processings: Maximum Likelihood and MUSIC (Multiple Signal Classification). The DORT-MUSIC algorithm gave the best results.

In an unpublished work [11], Devaney developed the formalism of DORT-MUSIC method, assuming isotropic scatterers. Special care was given to the maximum rank of the DORT matrix. Later, Lehman and Devaney [12] focused on the detection of point-like scatterers using DORT-MUSIC with two distinct arrays: one for the emission and one for the reception. In the same way, Miwa and Arai studied MUSIC algorithm in the case of the cross-borehole radar arrangement [13]. Baussard introduced a numerical method based on the recursively applied and projected (RAP) MUSIC to improve detection and localization of close targets [14]. Besides the early works, most of the surveys on this topic are theoretical and numerical. Along the few ones that are experimental, there is the Simonetti's work [15–17]. The aim was to resolve two 2 small holes with elastic surface waves or two small scattering with acoustic waves. Simonetti investigated the influence of multiple scattering on subwavelength imaging. However the first interpretation of the results [15] leads to a controversy [18]. In all these papers, scatterers are supposed to be isotropic: the rank of the problem is equal to the numbers of scatterers. Considering the two small elastic cylinders problem, Minonzio et al. showed the anisotropy of the scattering can modify greatly the singular values [19]. That is why scatterers, which scattering is experimentally isotropic, are considered in this paper.

The originality of this paper is twofold. First, no microwaves experiments have been performed with two close point-like scatterers. Second, thanks to the expansion of the singular vectors into power series with respect to the noise variance, the super-resolution limit is quantified. Concretely, a criterion describing the noise level above which the subwavelength resolution fails will be worked out. This criterion is very important experimentally to know if subwavelength resolution can be achieved.

After a brief description of the decomposition of the time reversal operator in Section 2, the experimental microwave setup is presented in details in Section 3. In Section 4, the experimental results are shown with two wires separated from less than half a wavelength.

We successfully resolve two copper wires, with $\lambda/200$ diameter and separated by $\lambda/6$. Section 5 is devoted to the development of the theoretical expressions of the Time Reversal Invariants obtained with two different antenna arrays: a transmit one and a receive one. In Section 6, thanks to a perturbation approach, the TRI are deduced in presence of external noise. Then the TRI are used to build up the projection operator that is the heart of the MUSIC method. The theoretical results are then compared to numerical simulations and to the experiment. It will be shown that the DORT-MUSIC subwavelength imaging imposes the noise to be inferior to a certain level given in this paper. From this study, a new resolution criterion is introduced.

2. TIME REVERSAL INVARIANTS AND SINGULAR VALUE DECOMPOSITION

In the present paper, as seen in several previous work [5, 12, 20, 21], DORT method is applied to distinct antenna arrays labelled A and B . The number of antennas of arrays A and B are equal to N^A and N^B , respectively. The receive vector \mathbf{R} on array B is linearly linked to the transmit vector \mathbf{E} on array A through the linear relation $\mathbf{R} = \mathbf{K}\mathbf{E}$. The $N^B \times N^A$ matrix \mathbf{K} is the frequency dependent matrix containing the inter-element response $k_{ij}(\omega)$ between element $\#j$ of the array A and element $\#i$ of the array B . After time reversal, i.e., phase conjugation of \mathbf{R} at one frequency, the signal is emitted back by array B to the array A . The signal received on array A writes $\mathbf{K}\mathbf{R}^*$ which is equal to $(\mathbf{K}^H \mathbf{K}\mathbf{E})^*$, where superscript $*$, T and H means conjugate, transpose and transpose-conjugate respectively. If array B emits first the signal \mathbf{E} , the receive signal on array B after time reversal by array A is $(\mathbf{K}\mathbf{K}^H \mathbf{E})^*$.

Two matrices $\mathbf{K}\mathbf{K}^H$ and $\mathbf{K}^H \mathbf{K}$ appear, the so-called Time Reversal Operators (TRO). They are diagonalizable because they are Hermitian. We write \mathbf{v}_j the j th eigenvector of $\mathbf{K}^H \mathbf{K}$ and \mathbf{u}_j the one of $\mathbf{K}\mathbf{K}^H$. These eigenvectors can be interpreted as the Invariants of the Time Reversal (TRI) process. For instance, after emission of \mathbf{v}_j by array A and time reversal by array B , the signals on array A is simply given by $\lambda_j^2 \mathbf{v}_j$. The time reversal invariants can be also directly worked out from the singular value decomposition (SVD) of the matrix \mathbf{K}

$$\mathbf{K} = \sum_{j=1}^{\min(N^A, N^B)} (\mathbf{u}_j) \lambda_j (\mathbf{v}_j)^H \quad (1)$$

Hence the singular vectors of matrix \mathbf{K} are the eigenvectors of the TRO. As for the singular values, they are the square root of the eigenvalues.

Practically speaking, the \mathbf{K} matrix is recorded between a transmit (Tx) array and a receive (Rx) array. The \mathbf{v}_j will hence be also referred as Tx singular vectors (or Tx-TRI) and the \mathbf{u}_j the Rx singular vectors (or Rx-TRI).

3. EXPERIMENTAL SETUP

In our experiments, the receiving array is linear and continuous. The emitting array is also linear but splits into two parts over the both sides of the receiving array (see Fig. 1). We will see further that this configuration is used to improve the imaging from the Rx Time Reversal Invariants.

Two horn antennas, which are 96 cm long and have a 58° aperture angle, move along the x -axis on a rail. The antennas are working between 2.6 GHz and 4 GHz. They are automated in rotation in order to take aim to the wires at each position. The response between the first and the second antenna is recorded on a vector spectral analyser with a frequency step of 87.5 kHz. To minimize parasitic echoes, the wall behind the wire is covered with anechoic material. The distance F

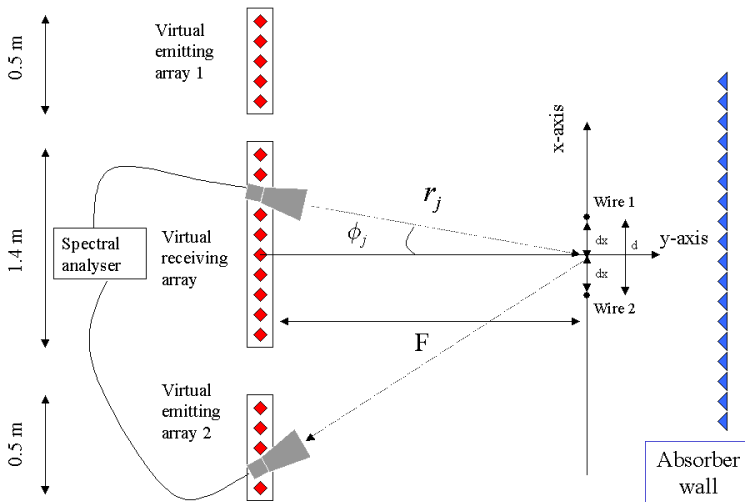


Figure 1. Experimental set-up.

from the rail on which the antennas are mounted to the wires is equal to 1.35 m. As the reception array aperture, denoted D , is of the same order as F , the resolution $\lambda F/D$ is about λ .

The scatterers consist of two copper wires with 0.6 mm diameter, corresponding to about $1/200\lambda$. The distance $2dx$ between the two wires is denoted d and ranges from $\lambda/10$ to $\lambda/4$.

4. EXPERIMENTAL RESULTS

4.1. Singular Values

To improve our results, the inter element responses of the medium without the wires are subtracted. Consequently the remaining parasitic echoes are therefore significantly reduced. The plot of the singular values on Fig. 2 lets appear a dominant one. The second singular value λ_2 increases with respect to frequency, whereas the third one λ_3 that keeps steady is attributed to noise. We will see that the ratio between the second singular value and the third one, i.e., λ_2/λ_3 , is a key parameter in order to perform sub-wavelength imaging.

4.2. Back-propagation of the Singular Vectors with the MUSIC Algorithm

The resolution of a simple (linear) match filtering method (such as beamforming) is limited to $\lambda/2$. So we choose a non-linear method, the MUSIC algorithm to resolve close wires. The MUSIC method requires

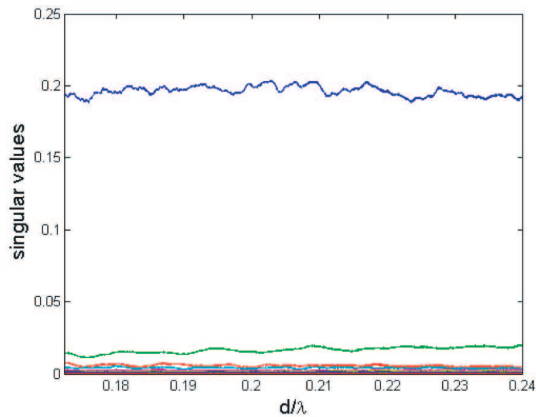


Figure 2. Experimental singular values λ_n for a distance between the two wires d equal to 22 mm.

the knowledge of the medium Green’s function. Considering the system as equivalent to a bi-dimensional one, the far field expression of the Green’s function can be approximated by

$$G(\mathbf{r}, \mathbf{r}') = \sqrt{\frac{2}{i\pi k |\mathbf{r} - \mathbf{r}'|}} e^{ik|\mathbf{r} - \mathbf{r}'|} \quad (2)$$

In the horizontal plane, the two wires are considered as pointlike and the field transmitted by the horn antennas is vertically polarized. As shown in the Appendix of [22], the scattering of a small metallic cylinder in E parallel polarization corresponds to the Dirichlet condition and it is equivalent to the acoustical soft boundary condition as an air bubble in water. It implies that for diameter small compared to the wavelength, the scattering is purely isotropic and non negligible.

In such a case, the dimension p of the signal subspace, i.e., the rank of \mathbf{K} , is equal to the number of scatterers. Here $p = 2$. The MUSIC estimator writes:

$$I_{MU}(r) = \frac{1}{1 - \sum_{n=1}^2 \left| \langle \mathbf{u}_n \mid \tilde{\mathbf{G}}(\mathbf{r}) \rangle \right|^2} \quad (3)$$

The vector $\tilde{\mathbf{G}}(\mathbf{r})$ stands for the normalized vector ($\mathbf{G}(\mathbf{r}) / \|\mathbf{G}(\mathbf{r})\|$) and the i th component of vector $\mathbf{G}(\mathbf{r})$ is given by $G(\mathbf{r}, \mathbf{r}_i)$. The antenna positions \mathbf{r}_j must be accurately known to be able to resolve close wire.

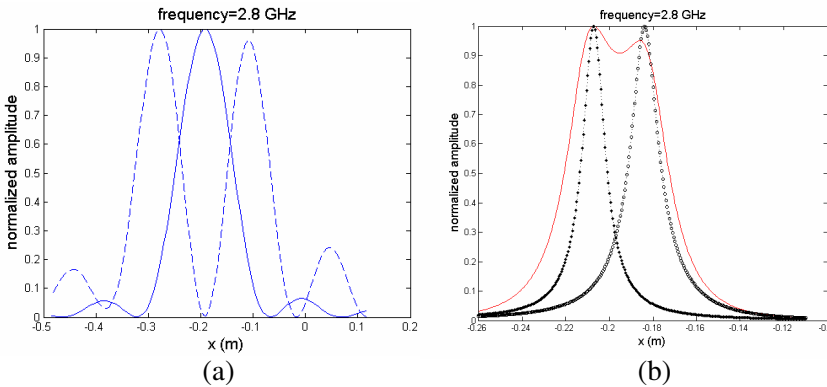


Figure 3. (a) Normalized classical back-propagation of the first singular vector (continuous) and the second one (dashed line). (b) Normalized MUSIC estimators obtained with the two first singular values in case of: Two wires (continuous line), left wire (dashed line) and right wire (circle).

In Fig. 3 are plotted the results of the MUSIC estimation obtained for 3 configurations: The left wire alone, the right wire alone and both of them. We see that MUSIC estimator enables to localize the wires that are spaced by $\lambda/3.5$.

At best, the resolution of wires separated by $d = \lambda/6$ is achieved. As it can be seen on Fig. 4, the smaller d is, the weaker the double maxima relative amplitude is.

To quantify the subwavelength resolution, we have plotted the MUSIC estimation computed on the x -axis versus λ/d (Fig. 5). While d/λ is large enough, it appears that the two wires are well resolved.

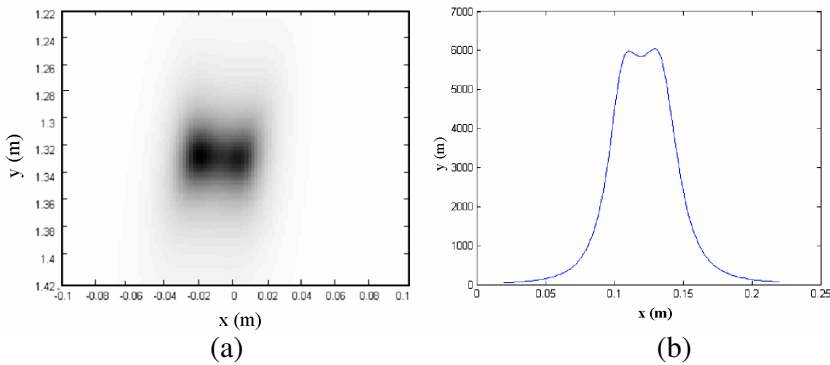


Figure 4. Imagined obtained with MUSIC, (a) $d = \lambda/5$, (b) $d = \lambda/6$ ($\lambda = 11.5$ cm here).

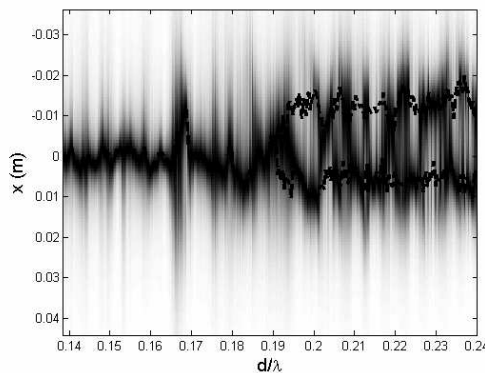


Figure 5. MUSIC algorithm projected on the x -axis with respect to d/λ for two wires separated of $d = 2$ cm.

Two spots appear on the image at the wires location. When d/λ decreases, the interpretation becomes less obvious. Above $(d/\lambda)_{\text{lim}} = 0.195$, the system is no more resolved and only one spot appears on the image, localized between the two wires.

The two wires are not resolved although the second singular value is still above the noise background. In the next sections, we propose a theoretical analysis to explain this effect.

5. THEORY: SINGULAR VALUE DECOMPOSITION OF \mathbf{K}

As the wires and the polarization of the antennas are both vertical, the problem is reduced to a two-dimensional scalar problem. The same formalism as in Ref. [19] is used. For the left wire alone, the rank of \mathbf{K} equals 1 and the SVD writes $\tilde{\mathbf{U}}_L \sigma \tilde{\mathbf{V}}_L^H$. The vectors $\tilde{\mathbf{V}}_L$ and $\tilde{\mathbf{U}}_L$ stands for the normalized propagation from the Tx-array to the left wire and the left wire to the Rx-array, respectively (i.e., $\tilde{G}(\mathbf{r}_i^{\text{Tx}}, \mathbf{r}_L)$ and $\tilde{G}(\mathbf{r}_L, \mathbf{r}_i^{\text{Rx}})$). Replacing L-subscript by R-subscript provides the expression for the right wire. The coefficient σ stands for the scattering coefficient of one wire multiplied by the norm of the propagating vectors [19]. When the two wires are in front of the arrays, the \mathbf{K} matrix is written

$$\mathbf{K} = \tilde{\mathbf{U}}_L \sigma \tilde{\mathbf{V}}_L^H + \tilde{\mathbf{U}}_R \sigma \tilde{\mathbf{V}}_R^H. \tag{4}$$

Here the multiple scattering between the wires is neglected. Taking it into account leads to

$$\mathbf{K} = \frac{1}{1 - (R_0 h)^2} \left(\tilde{\mathbf{U}}_L \sigma \tilde{\mathbf{V}}_L^H + \tilde{\mathbf{U}}_R \sigma \tilde{\mathbf{V}}_R^H + \tilde{\mathbf{U}}_L \sigma h R_0 \tilde{\mathbf{V}}_R^H + \tilde{\mathbf{U}}_R \sigma h R_0 \tilde{\mathbf{V}}_L^H \right), \tag{5}$$

where R_0 is the reflection coefficient of one wire and $h = \frac{e^{ikd}}{\sqrt{kd}}$ stands for Green's function between the two wires. The $N^{\text{Rx}} \times N^{\text{Tx}}$ matrix can be reduced to a problem of rank 2 (2 by 2 matrix). The two non-zero singular values of \mathbf{K} are given by

$$\begin{cases} \lambda_1 = |\sigma| \sqrt{1 + w_{LR}^{\text{Tx}} + w_{LR}^{\text{Rx}} + w_{LR}^{\text{Tx}} w_{LR}^{\text{Rx}}} \left| \frac{1}{1 - R_0 h} \right| \\ \lambda_2 = |\sigma| \sqrt{1 - w_{LR}^{\text{Tx}} - w_{LR}^{\text{Rx}} + w_{LR}^{\text{Tx}} w_{LR}^{\text{Rx}}} \left| \frac{1}{1 + R_0 h} \right| \end{cases}. \tag{6}$$

They are associated with the singular vectors:

$$\begin{cases} \mathbf{u}_1 \approx \frac{(\tilde{\mathbf{U}}_L + \tilde{\mathbf{U}}_R)}{\|\tilde{\mathbf{U}}_L + \tilde{\mathbf{U}}_R\|} \\ \mathbf{u}_2 \approx \frac{(\tilde{\mathbf{U}}_L - \tilde{\mathbf{U}}_R)}{\|\tilde{\mathbf{U}}_L - \tilde{\mathbf{U}}_R\|} \end{cases} \tag{7}$$

In Eq. (6), the term w_{LR}^{Tx} (resp. w_{LR}^{Rx}) stands for the scalar products between $\tilde{\mathbf{V}}_L$ and $\tilde{\mathbf{V}}_R$ (resp. $\tilde{\mathbf{U}}_L$ and $\tilde{\mathbf{U}}_R$). As the distance between the two wires decreases, w_{LR}^{Rx} and w_{LR}^{Tx} increase towards 1. As a result, the first singular value increases and the second one decreases. Hence, the second one can be very sensitive to noise, which degrades the quality of the imaging. As the wires are considered to be in the far field from the arrays,

$$\left\{ \tilde{\mathbf{U}}_L \right\}_j = \frac{1}{\sqrt{N^{Tx}}} e^{ikr_{jL}^{Rx}} \tag{8}$$

where r_{jL}^{Rx} is the distance for Rx-antenna # j and the left wire. Same expressions are obtained for the right wire and the Tx-array. In the following the Rx superscript is omitted because only the Rx-array is considered. In Eq. (8), the aperture of the antennas is not taken into account because the antennas take aim to the wires location. Thanks to the symmetric configuration of the receiving array (Fig. 6), the positions are well approximated by

$$\begin{cases} r_{Rj} \approx r_j - dx \sin(\phi_j) \\ r_{Lj} \approx r_j + dx \sin(\phi_j) \end{cases} \tag{9}$$

From Eqs. (7) and (9) the singular vectors can then be written

$$\begin{cases} u_{1j} = \frac{1}{\|\tilde{\mathbf{U}}_L + \tilde{\mathbf{U}}_R\|} e^{ikr_j} \cos(kdx \sin(\phi_j)) \\ u_{2j} = \frac{1}{\|\tilde{\mathbf{U}}_L - \tilde{\mathbf{U}}_R\|} e^{ikr_j} \sin(kdx \sin(\phi_j)) \end{cases} \tag{10}$$

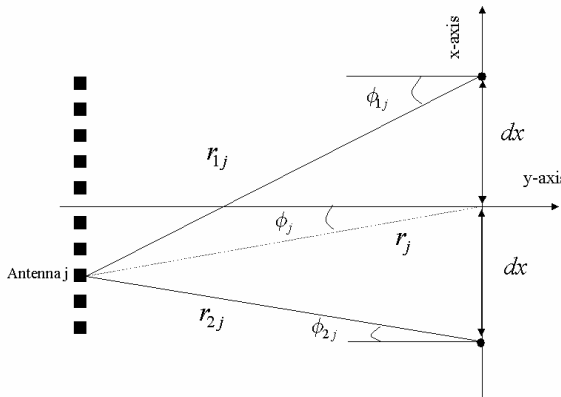


Figure 6. Experimental configuration of the Tx-array in front of the two wires that are $2dx$ distant.

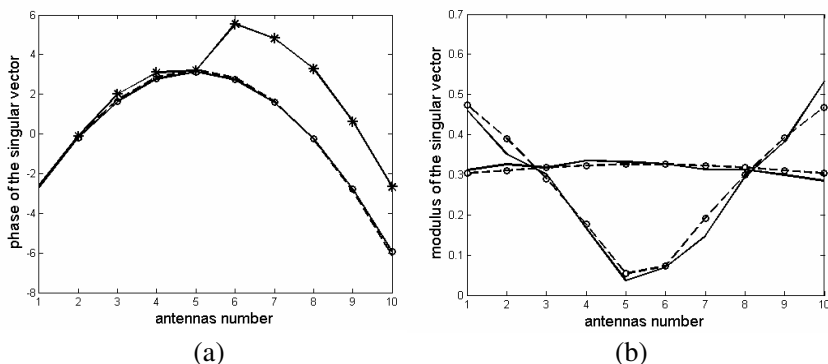


Figure 7. (a) Experimental phase of the first (o marker, continuous line) and second (* marker, continuous line) singular vectors, and theoretical $-kr_j$ (dash line), (b) modulus of the first and second singular vectors, theoretical (dashed line, o marker) and experimental (continuous).

Figure 7 shows a good fit between the experimental and theoretical singular vectors given by Eq. (10). Due to the orthogonality between the singular vectors, the second vanishes with a π phase shift, between the 5th and the 6th antenna.

Nevertheless, a slight mismatch between theoretical and experimental singular values can completely degrade the MUSIC technique. To estimate how fast is the degradation; we will assume that it is mainly due to external noise on the measurement of \mathbf{K} matrix. Hence in the next section, using a Taylor expansion, the singular vectors are theoretically computed.

6. PERTURBATION THEORY ON SINGULAR VECTORS

In this part, the sensitivity of the DORT-MUSIC method to noise will be quantitatively discussed for subwavelength resolution. Theoretically, without noise, the MUSIC estimator diverges on the two wires locations, whatever the distance between them. It implies that the two wires are in this ideal case always resolved with DORT-MUSIC method, even for very close wires. However, for any small perturbation, the MUSIC estimator remains finite and the resolution is therefore not systematically achieved. To quantify the effect, we analytically estimates Eq. (3) in the case of a white Gaussian noise of variance σ_B that perturbs the \mathbf{K} matrix measurement. The singular

vectors are expanded in Taylor's series of the noise variance. The aim is to work out an analytical expression of the noise level above which the MUSIC estimator fails to resolve the wires. In fact, contrary to what one would expect at first thought, the subwavelength resolution of the two wires does not always occur when the second signal singular value is higher than the third one associated to noise. We will show that, in the far field limit, an explicit criterion between those two singular values can be worked out in order to achieve subwavelength imaging.

To validate the theoretical expressions, they are compared to simple numerical simulations developed under Matlab. In the numerical simulations, the propagation between the antennas and the wires are modelled by the Green's function. The scattering coefficients of the two wires are equal. An additive white Gaussian noise is added to the \mathbf{K} matrix. The number of antennas of the emitting and receiving arrays is chosen to be large enough to allow a statistical approach ($N^{\text{Rx}} = N^{\text{Tx}} = N = 100$). The wavelength λ equals 0.1 m. The distance between the wires is noted d , with $d = 2dx$, and the noise variance σ_B^2 . The aperture D of the receiving array is 0.2 m, and the wires are located at a distance $F = 5$ m from the arrays. The distance between the wires varies between $\lambda/10$ and $\lambda/2$ in the simulations.

6.1. Expansion of the Singular Values into Convergent Power Series

Consider the previous theoretical matrix \mathbf{K} perturbed by a noise random matrix:

$$\mathbf{K}^p = \mathbf{K} + \sigma_B \Delta \mathbf{K} = \sum_{i=1}^2 (\mathbf{u}_i) \lambda_i (\mathbf{v}_i)^{\mathbf{H}} + \sigma_B \Delta \mathbf{K} \quad (11)$$

From now a p superscript indicates perturbed values to distinguish them from their unperturbed values. The matrix $\Delta \mathbf{K}$ is a random matrix. Its Frobenius norm equals 1. By definition, the Frobenius norm of a matrix \mathbf{A} is given by:

$$\|\mathbf{A}\|_F = \sqrt{\sum_{i,j} |A_{ij}|^2} \quad (12)$$

Similarly to Eq. (11), the SVD of \mathbf{K} is given by

$$\mathbf{K}^p = \sum_{i=1}^N (\mathbf{u}_i^p) \lambda_i^p (\mathbf{v}_i^p)^{\mathbf{H}} \quad (13)$$

In this section the singular vectors of \mathbf{K}^p will be established in order to use them, in the next section, in the MUSIC estimator. The

perturbation analysis on singular vectors and singular values has been well documented in literature [23–27]. The perturbation of the singular vectors that span the signal subspace was especially established at first and second order [24, 25].

Due to the noise perturbation, the singular vectors can be expanded into convergent power series of the noise variance. Developed at the second order in small parameter σ_B , the singular vectors of the perturbed matrix \mathbf{K}^p can be written as:

$$\mathbf{u}_i^p = \mathbf{u}_i + \sigma_B \mathbf{w}_i^{(1)} + \sigma_B^2 \mathbf{w}_i^{(2)} + o(\sigma_B^2) \quad (1 \leq i \leq 2) \quad (14)$$

The approximation made to develop the singular vectors into power series and the expression of the vectors \mathbf{w}_1 and \mathbf{w}_2 are given in Appendix A. The expected (mean) values of their different components are also expressed. Their expected values will be used in the following to estimate the mean perturbation on the MUSIC estimator.

When the wires are close, we have seen that the first singular value is much bigger than second one. As a result, according to the expression provided par Jun et al. [26], the expected perturbation on the first singular vector is roughly null at the second order:

$$\mathbf{u}_1^p \simeq \mathbf{u}_1 + o(\sigma_B^2) \quad (15)$$

Only the perturbation on the second singular vector will then significantly modify the MUSIC estimator.

6.2. Application to the MUSIC Estimator

To simplify the results of the MUSIC algorithm, let us define the L function as:

$$L(\tilde{\mathbf{G}}(\mathbf{r})) = \left| \langle \mathbf{u}_1^p \mid \tilde{\mathbf{G}}(\mathbf{r}) \rangle \right|^2 + \left| \langle \mathbf{u}_2^p \mid \tilde{\mathbf{G}}(\mathbf{r}) \rangle \right|^2. \quad (16)$$

L represents the square of the distance of $\tilde{\mathbf{G}}$ from the subspace built from \mathbf{u}_1 and \mathbf{u}_2 . Then the MUSIC estimator becomes:

$$I_{MU}(\tilde{\mathbf{G}}(\mathbf{r})) = \frac{1}{1 - L(\tilde{\mathbf{G}}(\mathbf{r}))} \quad (17)$$

The I_{MU} estimator only increases the contrast of the L estimator thanks to a strong non-linear relation. In the upcoming calculations, we use $\tilde{\mathbf{U}}_L$, $\tilde{\mathbf{U}}_R$ as in the previous section. Furthermore, we define $\tilde{\mathbf{U}}_M$ as the propagating vector between the receiving array and the position exactly between the two wires. Indeed, we will show that the wires are not anymore resolved when the expected value on the wires becomes inferior to the expected value between the wires.

The vector $\tilde{\mathbf{U}}_L$ can be expressed in terms of the signal subspace $\{\mathbf{u}_1, \mathbf{u}_2\}$ as:

$$\tilde{\mathbf{U}}_L = \frac{1}{2} \left(\mathbf{u}_1 \left\| \tilde{\mathbf{U}}_L + \tilde{\mathbf{U}}_R \right\| + \mathbf{u}_2 \left\| \tilde{\mathbf{U}}_L - \tilde{\mathbf{U}}_R \right\| \right) \quad (18)$$

with $\left\| \tilde{\mathbf{U}}_L + \tilde{\mathbf{U}}_R \right\| = \sqrt{2(1+w)}$ and $\left\| \tilde{\mathbf{U}}_L - \tilde{\mathbf{U}}_R \right\| = \sqrt{2(1-w)}$. The scalar w stands for the scalar cross product between $\tilde{\mathbf{U}}_L$ and $\tilde{\mathbf{U}}_R$, w is real in the far field approximation.

The expected value of the estimator L applied to the vectors $\tilde{\mathbf{U}}_L$ can now be calculated. The first order perturbation has no effect on the mean value of L . The expected value of L is computed at the second order in Appendix A. It leads to

$$E \left[L \left(\tilde{\mathbf{U}}_L \right) \right] = \frac{1+w}{2} + \frac{1-w}{2} \left(1 - \frac{(N-2)\sigma_B^2}{\lambda_2^2} \right) + o(\sigma_B^2). \quad (19)$$

The expected value of $L(\tilde{\mathbf{U}}_L)$ decreases from 1 when noise increases. Between the two wires, the contribution of the second singular vector, associated to an antisymmetric field, is null, so $L(\tilde{\mathbf{U}}_M)$ is given by:

$$E \left[L \left(\tilde{\mathbf{U}}_M \right) \right] = \left| \left\langle \mathbf{u}_1 \mid \tilde{\mathbf{U}}_M \right\rangle \right|^2 \quad (20)$$

To express the third singular value, one should use some results of the random matrix theory. Assuming the noise completely decorrelated from antenna to antenna, the singular values λ_n of which index is larger than 2 are the same ones, in a statistical point of view, as the ones of a $(N-2) * (N-2)$ random matrix. The quadrant law gives the distribution of the singular values of such a matrix. Especially, the largest singular value (i.e., λ_3), is given by:

$$\lambda_3 = 2\sqrt{N-2}\sigma_B \quad (21)$$

Fig. 8 displays the evolution of the L estimator for $\tilde{\mathbf{U}}_M$ and for $\tilde{\mathbf{U}}_L$ with respect to λ_3/λ_2 . The analytical formula in Eq. (19) fits the simulated curve very well.

The standard deviation normalized by the mean value of $L(\tilde{\mathbf{U}}_L)$ is small compared to its expected value (roughly equal to λ_2/λ_1). As a consequence, its value in one experimental measurement will be close to the analytical expected value.

In Paragraph 6.4, the threshold value of λ_3 above which the wires are not anymore resolved will be worked out.

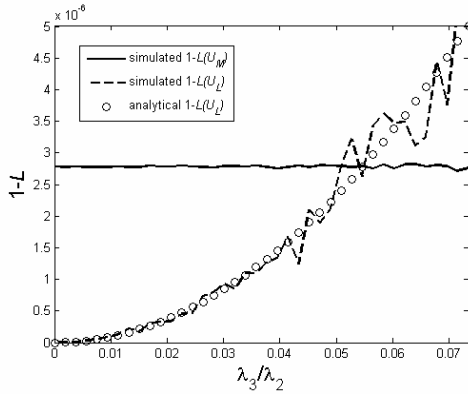


Figure 8. Simulated $1 - L(\tilde{\mathbf{U}}_M)$ (continuous) and $1 - L(\tilde{\mathbf{U}}_L)$ (dots) compared to the analytical formula in (19) (markers). The simulation parameter d is: $d = 0.39\lambda$.

6.3. Estimated Profile

We can also predict the expected profile of the DORT-MUSIC estimator between the two wires. For a point of coordinates $\mathbf{r} = [x, F]$, the vector $(\tilde{\mathbf{U}}_x)_i = \frac{e^{ik(r_i - x \sin(\phi_i))}}{\sqrt{N}}$ is very close to $\tilde{\mathbf{U}}_L$ and $\tilde{\mathbf{U}}_R$. Consequently, when computing $E[L(\tilde{\mathbf{U}}_\delta)]$, the contribution to the scalar products in (16) mainly comes from the components \mathbf{u}_1 and \mathbf{u}_2 (the signal sub-space) of Eq. (14). We neglect in particular the contribution of the noise subspace perturbation in $|\langle \tilde{\mathbf{U}}_x | \mathbf{u}_2^p \rangle|^2$.

In such a case, assuming that the wires are in the far-field and that the array aperture and the step between two antenna positions are sufficiently small, the L estimator writes from Appendix B:

$$\begin{aligned}
 & E \left[L \left(\tilde{\mathbf{U}}_x \right) \right] \\
 &= \frac{1}{2(1 + \text{sinc}(kdxD/F))} \left[\text{sinc} \left(\frac{k(dx-x)D}{2F} \right) + \text{sinc} \left(\frac{k(dx+x)D}{2F} \right) \right]^2 \\
 &+ \frac{1}{2(1 - \text{sinc}(kdxD/F))} \left[\text{sinc} \left(\frac{k(dx-x)D}{2F} \right) - \text{sinc} \left(\frac{k(dx+x)D}{2F} \right) \right]^2 \left(1 - \frac{\lambda_3^2}{4\lambda_2^2} \right)
 \end{aligned} \tag{22}$$

This formula is consistent with the expected values computed previously. Using Eq. (22), the DORT-MUSIC image can be built. The comparison between numerical simulation and the theoretical shape confirms the validity of our approach.

The theoretical I_{MU} is also compared to the experimental results in Fig. 10.

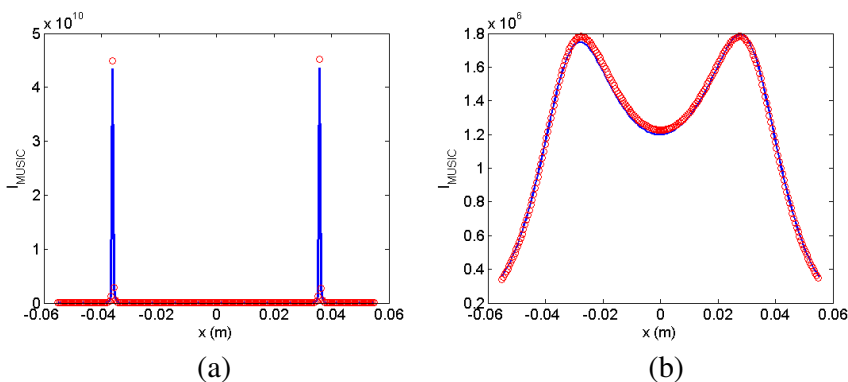


Figure 9. DORT-MUSIC estimator for two 0.36λ distant wires: Simulation (continuous line) and analytical expression from Eq. (22) (dots). Figure (a) is obtained without noise and (b) with $\lambda_3/\lambda_2 = 0.36$.

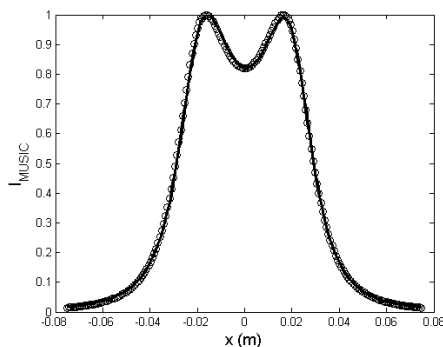


Figure 10. DORT-MUSIC estimator analytical expression from Eq. (22) (circles) with $\lambda_3/\lambda_2 = 0.24$ and experimental result (continuous line) for $\lambda_3/\lambda_2 = 0.22$. The distance between the wires is $d = 0.3\lambda$.

The agreement with the theory is excellent when the ratio λ_3/λ_2 in Eq. (22) is set to 0.24. This ratio is a little bit higher than the 0.22 experimental one. This result can be explained by the mismatch between the idealized model and the real experiment (such as antenna location, wave polarization, 2D assumption, etc.) This mismatch induces some “virtual” noise which has to be added to the measure noise. The experimental estimator corresponds then to a lightly superior white noise level.

6.4. Criterion to Resolve the System, Resolution Limit in Presence of Noise

To finish, from a given noise level, the expected value of L on the wires becomes inferior to the value between the wires. The subwavelength resolution cannot then be achieved because only one peak appears on the image. A resolution criterion can then be introduced:

$$E \left[L \left(\tilde{\mathbf{U}}_L \right) \right] > E \left[L \left(\tilde{\mathbf{U}}_M \right) \right]. \tag{23}$$

Using Eqs. (19), (20) and (21), the ratio between the third and the second singular value providing the super-resolution limit becomes

$$\frac{\lambda_3}{\lambda_2} \leq \frac{\lambda_3}{\lambda_2} \Big|_{\text{lim}} \simeq 2 \sqrt{\frac{2 \left(1 - \langle \mathbf{u}_1 | \tilde{\mathbf{U}}_M \rangle^2 \right)}{1 - w}}. \tag{24}$$

However, the expression in Eq. (24) is very general. Assuming the same small aperture hypothesis used in the previous section, we show in Appendix C that Eq. (24) is simplified into

$$\frac{\lambda_3}{\lambda_2} \Big|_{\text{lim}} = \frac{\pi}{\sqrt{15}} \frac{D}{F} \frac{d}{\lambda} + o \left(\frac{D}{F} \frac{d}{\lambda} \right). \tag{25}$$

This linear evolution is displayed in Fig. 11, where the expression in (25) is compared to numerical simulations.

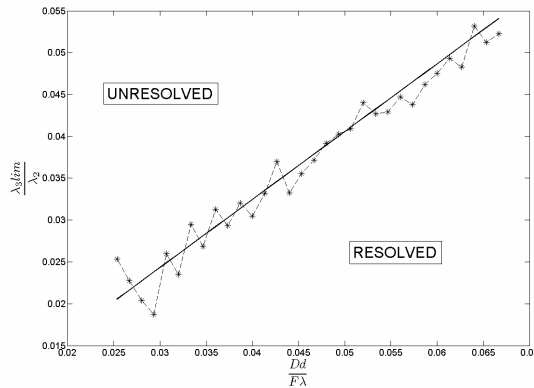


Figure 11. Simulated (markers) and analytical (continuous line) ratios $\frac{\lambda_3}{\lambda_2} \Big|_{\text{lim}}$ with respect to $\frac{D}{F} \frac{d}{\lambda}$.

Equation (25) leads to quantify the noise level above which the subwavelength resolution fails. The main result is that the super-resolution is not achieved when the criterion is not verified even if the second singular value is higher than third one. Indeed the second singular vectors can be too much perturbed in order to achieve subwavelength resolution. Hence, the DORT-MUSIC algorithm is then very sensitive to noise. However, for a distance between the wires close to or larger than $\lambda/2$, the super-resolution limit ratio is close to 1, that means the two wires are resolved as soon as the second singular value emerges from the noise background.

7. DISCUSSION

From Eq. (4), we deduce the transfer response between antenna $\#i$ and $\#j$ in a free space medium:

$$K_{ij} = 2 \frac{e^{ik(r_i^{\text{Tx}} + r_j^{\text{Rx}})}}{r_i^{\text{Tx}} r_j^{\text{Rx}}} \cos \left(kdx \left(\frac{X_i^{\text{Rx}}}{F} + \frac{X_j^{\text{Tx}}}{F} \right) \right) \quad (26)$$

Here, for simplicity, we neglect multiple scattering. The phase of the response K_{ij} in Eq. (26) only depends on the barycentre of the wires while the distance dx between them only affects the amplitude term through the cosine function. Integrating this cosinus function over the whole array aperture lets appear a sinc function of the distance dx divided by the resolution cell $\lambda F/D$. This integral is used to calculate the scalar product w developed in Appendix B, Eq. (41), which is a key parameter for resolution. As the slope of the sinc function varies linearly with dx , the sensitivity to a variation of dx also decreases linearly with dx . This fact explains the difficulty to separate close targets. As shown in Eq. (25), the smaller the distance between the wires is, the more sensitive the DORT-MUSIC estimator becomes.

Concretely, two concomitant effects explain this consideration. First, the second singular value decreases when the wires become close, because the scalar product w increases and becomes close to 1 (see Eq. (6)). Second, for a small distance between the wires, following the criterion in Eq. (25), the second singular value should be much larger than the third one. To understand this point, if we used a classical beam-forming method for each wires, the two focal spots would overlap and the level between them would increase when d decreases. The DORT-MUSIC method overcomes this difficulty by the way of a strongly non-linear relation. However, the drawback is the dramatic sensitivity to noise. The subwavelength resolution in presence of noise becomes thus all the more difficult to achieve that d is small.

Note that the perturbation theory on the singular vectors is still valid whether multiple scattering occurs between the wires. Without noise, single scattering and multiple scattering singular vectors are the same. With noise, multiple scattering can either increase or decrease the second singular value. Simonetti et al. proposed that multiple scattering can be really helpful in case of large noise levels [17]. In fact, in the case of the DORT-MUSIC method, multiple scattering will only change the singular values. The interaction between the noise level and the associated singular vectors used to image the scatterers is then a key point to achieve super-resolution. As the criterion is still valid, multiple scattering will either improve or degrade the resolution limit.

In DORT-MUSIC method, a key point concerns the number of singular vectors that are taken into account in the signal subspace. It has been shown that including the first noise singular vectors can improve the DORT-MUSIC. Prada et al. observed that the performance of the MUSIC algorithm could be improved by selecting the first seven singular vectors [10], for an emitting-receiving array of 128 transducers. Experimentally, we observed a similar phenomenon, whereas the number of antennas was much smaller ($N = 10$). But those noise singular vectors that improved the resolution were not necessarily the same at each frequency. In fact, the singular vectors \mathbf{u}_k^p , $k > 2$, of the perturbed matrix \mathbf{K}^p depend also on the 2 singular vectors of the unperturbed matrix \mathbf{K} . Hence the noise subspace contains also useful information. This fact explains that including more singular vectors can improve the DORT-MUSIC performances. A future work will consist in studying the resolution property of the DORT method combined with other estimators such as minimum variance or white noise constrained where all the singular vectors are taken into account with different weight for each of them.

8. CONCLUSION

This study results from the need to interpret experimental results obtained with the DORT-MUSIC method applied to two close metallic wires. Hence, the efficiency of the DORT method to image a subwavelength system of two small scatterers has been proved. This study is based on the analysis of the singular vectors in terms of Taylor power series. From this analysis, the performance of the DORT-MUSIC method has been studied in details. Special care has been given to the limit of the method in terms of signal to noise ratio. Especially it has been shown that even if the second singular value is larger than the noise singular values, it might be still impossible to

resolve the two wires. Our approach has been validated numerically and experimentally.

ACKNOWLEDGMENT

This work was financially supported by the French Army, DGA/MRIS, under the grant REI — AORTE — #0634002.

APPENDIX A.

Considering that the expansion in power series is valid for

$$E [\|\sigma_B \Delta \mathbf{K}\|_F] \ll \left\| \sum_{i=1}^2 (\mathbf{u}_i) \lambda_i (\mathbf{v}_i)^H \right\|_F,$$

it means that the second order perturbation holds true as long as:

$$N \sigma_B \ll \sqrt{\lambda_1^2 + \lambda_2^2} \quad (\text{A1})$$

As we are interested in configurations where the distance between the wires is small compared to the wavelength, the second singular value λ_2 is small compared to the first singular value. The noise variance is also considered as inferior to the second singular value but of the same order: $\lambda_1 \gg \lambda_2 > \sigma_B$. In such a case, an other hypothesis is done in the following calculations:

$$\frac{\lambda_1^2 + \lambda_2^2}{(\lambda_1^2 - \lambda_2^2)^2} \simeq \frac{1}{\lambda_1^2} \ll \frac{N-2}{\lambda_2^2} \quad (\text{A2})$$

According to the SVD properties (projection on signal subspace and orthogonality of the new singular vectors), the first order perturbation is given by:

$$\begin{aligned} \mathbf{w}_1^{(1)} &= \frac{\mathbf{u}_2^H (\Delta \mathbf{K} \mathbf{K}^H + \mathbf{K} \Delta \mathbf{K}^H) \mathbf{u}_1}{\lambda_1^2 - \lambda_2^2} \mathbf{u}_2 \\ &+ \sum_{k=3}^N \frac{\mathbf{u}_k^H (\Delta \mathbf{K} \mathbf{K}^H + \mathbf{K} \Delta \mathbf{K}^H) \mathbf{u}_1}{\lambda_1^2} \mathbf{u}_k \end{aligned} \quad (\text{A3})$$

$$\begin{aligned} \mathbf{w}_2^{(1)} &= \frac{\mathbf{u}_1^H (\Delta \mathbf{K} \mathbf{K}^H + \mathbf{K} \Delta \mathbf{K}^H) \mathbf{u}_2}{\lambda_2^2 - \lambda_1^2} \mathbf{u}_1 \\ &+ \sum_{k=3}^N \frac{\mathbf{u}_k^H (\Delta \mathbf{K} \mathbf{K}^H + \mathbf{K} \Delta \mathbf{K}^H) \mathbf{u}_2}{\lambda_2^2} \mathbf{u}_k \end{aligned} \quad (\text{A4})$$

Vectors $\mathbf{w}_1^{(1)}$ and $\mathbf{w}_2^{(1)}$ are composed of two contributions: the first one stands for the contribution of the signal subspace (generated by \mathbf{u}_1 and \mathbf{u}_2), whereas the second one for the contribution of the “noise” subspace. This last one is responsible of the degradation of the MUSIC estimator.

Considering the expected value of their components, Jun Liu et al. in [26] showed that:

$$E \left[\left\langle \mathbf{w}_2^{(1)} | \mathbf{u}_1 \right\rangle \right] = 0 \tag{A5}$$

$$E \left[\left\| \left\langle \mathbf{w}_2^{(1)} | \mathbf{u}_1 \right\rangle \mathbf{u}_1 \right\|^2 \right] = \frac{\lambda_1^2 + \lambda_2^2}{(\lambda_1^2 - \lambda_2^2)^2} \approx 0 \tag{A6}$$

$$E \left[\left\| \sum_{k=3}^N \left\langle \mathbf{w}_2^{(1)} | \mathbf{u}_k \right\rangle \mathbf{u}_k \right\|^2 \right] = \frac{N - 2}{\lambda_2^2}, \tag{A7}$$

where E stands for the expected value (mean). Due to the approximation made in Eq. (A2), the expected signal subspace contribution on the second singular vectors perturbation in Eq. (A6) is far less than the one of the noise subspace, expressed in Eq. (A7).

The second order expansions of \mathbf{u}_1^p and \mathbf{u}_2^p are much more complex. The exact expression of the second order perturbation is given in reference [25]. Nevertheless $\mathbf{w}_1^{(2)}$ and $\mathbf{w}_2^{(2)}$ can be expressed in terms of the \mathbf{u}_k vectors:

$$\mathbf{w}_i^{(2)} = \sum_{k=1}^N a_{ki} \mathbf{u}_k \tag{A8}$$

For the second singular vector, the two first coefficients at the second order are:

$$a_{12} = \frac{\lambda_1 \mathbf{u}_1^H \Delta \mathbf{K} \mathbf{w}_2^{(1)} + \lambda_2 \mathbf{u}_1^H \Delta \mathbf{K}^H \mathbf{w}_2^{(1)} - (\lambda_1 c_1 + \lambda_2 c_2)}{\lambda_2^2 - \lambda_1^2} \tag{A9}$$

$$a_{22} = -\frac{1}{2} \left(\mathbf{w}_2^{(1)H} \mathbf{w}_2^{(1)} \right) \tag{A10}$$

where c_1 and c_2 in Eq. (A9) stands for two coefficients verifying $E[c_k] = 0$ ($1 \leq k \leq 2$). The other coefficients are not necessary to apply the MUSIC estimator.

Their expected values become:

$$E[a_{12}] \simeq 0 \text{ and } E[a_{22}] = -\frac{1}{2} \frac{N - 2}{\lambda_2^2} \tag{A11}$$

In order to apply the MUSIC algorithm, the norm of the perturbed singular vectors at the second order has to equal 1. If the norm of the first singular vector is obvious, concerning the second one, it verifies:

$$\begin{aligned} \|\mathbf{u}_2^p\|^2 &= (\mathbf{u}_2^p | \mathbf{u}_2^p) \\ &= \langle \mathbf{u}_2 | \mathbf{u}_2 \rangle + 2\sigma_B \langle \mathbf{w}_2^{(1)} | \mathbf{u}_2 \rangle \\ &\quad + \sigma_B^2 \left(\|\mathbf{w}_2^{(1)}\|^2 + 2 \langle \mathbf{w}_2^{(2)} | \mathbf{u}_2 \rangle \right) + o(\sigma_B^2) \end{aligned} \quad (\text{A12})$$

As $\{\mathbf{u}_k\}$ constitutes an orthonormal basis and due to Eq. (33) and Eq. (37), it becomes:

$$\|\mathbf{u}_2^p\|^2 \simeq 1 + o(\sigma_B^2) \quad (\text{A13})$$

The two wires are then well orthogonal and normalized, even at the second order.

APPENDIX B.

If the wires are in the far field and the array pitch sufficiently small, the scalar product between $\tilde{\mathbf{U}}_L$ and $\tilde{\mathbf{U}}_R$ becomes:

$$w \approx \frac{1}{N} \int_{-D/2}^{D/2} e^{2ikdx \frac{s}{F}} \frac{ds}{p}, \quad (\text{B1})$$

The integration is done along the x -axis, but we use the index s for not confounding with the distance dx . It leads to:

$$w \approx \text{sinc} \left(\frac{kdD}{2F} \right). \quad (\text{B2})$$

Moreover, in the same way, the expected value of the scalar products between the singular vectors and $\tilde{\mathbf{U}}_\delta$ can be computed:

$$E \left[\left| \langle \mathbf{u}_1^p | \tilde{\mathbf{U}}_x \rangle \right|^2 \right] = \left(\sqrt{\frac{2}{1+w}} \int_{-D/2}^{D/2} \frac{\cos(kdx \frac{s}{F}) e^{-ikx \frac{s}{F}} ds}{N} \frac{ds}{p} \right)^2 \quad (\text{B3})$$

which gives:

$$\begin{aligned} &E \left[\left| \langle \mathbf{u}_1^p | \tilde{\mathbf{U}}_x \rangle \right|^2 \right] \\ &= \frac{1}{2(1+w)} \left[\text{sinc} \left(\frac{k(dx-x)D}{2F} \right) + \text{sinc} \left(\frac{k(dx+x)D}{2F} \right) \right]^2 \end{aligned} \quad (\text{B4})$$

In the same way,

$$\begin{aligned}
 & E \left[\left| \langle \mathbf{u}_2^p | \tilde{\mathbf{U}}_x \rangle \right|^2 \right] \\
 &= \left(1 - \frac{\lambda_3^2}{4\lambda_2^2} \right) \left(\sqrt{\frac{2}{(1-w)}} \int_{-D/2}^{D/2} \frac{\sin(kdx \frac{s}{F}) e^{-ikx \frac{s}{F}}}{N} ds \right)^2 \quad (B5)
 \end{aligned}$$

which results to

$$\begin{aligned}
 & E \left[\left| \langle \mathbf{u}_2^p | \tilde{\mathbf{U}}_x \rangle \right|^2 \right] \\
 &= \frac{1}{2(1-w)} \left[\text{sinc} \left(\frac{k(dx-x)D}{2F} \right) - \text{sinc} \left(\frac{k(dx+x)D}{2F} \right) \right]^2 \left(1 - \frac{\lambda_3^2}{4\lambda_2^2} \right) \quad (B6)
 \end{aligned}$$

Finally, it leads to

$$\begin{aligned}
 & E \left[L \left(\tilde{\mathbf{U}}_x \right) \right] \\
 &= \frac{1}{2(1+w)} \left[\text{sinc} \left(\frac{k(dx-x)D}{2F} \right) + \text{sinc} \left(\frac{k(dx+x)D}{2F} \right) \right]^2 \\
 &+ \frac{1}{2(1-w)} \left[\text{sinc} \left(\frac{k(dx-x)D}{2F} \right) - \text{sinc} \left(\frac{k(dx+x)D}{2F} \right) \right]^2 \left(1 - \frac{\lambda_3^2}{4\lambda_2^2} \right) \quad (B7)
 \end{aligned}$$

This formula gives the expected profile between the two wires.

APPENDIX C.

First we remain that the scalar product of the first singular value of the vector of the point between the wires is:

$$\langle \mathbf{u}_1 | \tilde{\mathbf{U}}_0 \rangle \approx \sqrt{\frac{2}{1+w}} \text{sinc} \left(kdx \frac{D}{2F} \right) \quad (C1)$$

Using Eq. (24) and Eq. (C1), the threshold ratio giving the resolution criterion in (24) becomes:

$$\left. \frac{\lambda_3}{\lambda_2} \right|_{\text{lim}} = 2 \sqrt{\frac{2 \left\{ 1 - 2 \left[\text{sinc} \left(kdx \frac{D}{2F} \right) \right]^2 / \left[1 + \text{sinc} \left(kdx \frac{D}{F} \right) \right] \right\}}{1 - \text{sinc} \left(kdx \frac{D}{F} \right)}} \quad (C2)$$

By developing the sinc function at the fourth order with respect to $(kdx \frac{D}{F})$, we finally obtain:

$$\left. \frac{\lambda_3}{\lambda_2} \right|_{\text{lim}} = \frac{2\pi}{\sqrt{15}} \frac{D}{F} \frac{dx}{\lambda} + o \left(\frac{D}{F} \frac{dx}{\lambda} \right) \quad (C3)$$

REFERENCES

1. Cheney, M., "The linear sampling method and the MUSIC algorithm," *Inverse Problems*, Vol. 17, 591–595, 2001.
2. Lev-Ari, H. and A. J. Devaney, "The time-reversal technique re-interpreted: Subspace-based signal processing for multi-static target location," *Sensor Array and Multichannel Signal Processing Workshop, 2000, Proceedings of the 2000 IEEE*, 509–513, 2000.
3. Prada, C. and M. Fink, "Eigenmodes of the time reversal operator: A solution to selective focusing in multiple-target media," *Wave Motion*, Vol. 20, 151–163, 1994.
4. Kerbrat, E., R. K. Ing, C. Prada, D. Cassereau, and M. Fink, "The D. O. R. T. method applied to detection and imaging in plates using Lamb waves," *Review of Progress in Quantitative Nondestructive Evaluation*, 934–940, Ames, Iowa (USA), 2001.
5. Prada, C., M. Tanter, and M. Fink, "Flaw detection in solid with the D. O. R. T. method," *Ultrasonics Symposium*, Vol. 1, 679–683, 1997.
6. Kerbrat, E., D. Clorennec, C. Prada, D. Royer, D. Cassereau, and M. Fink, "Detection of cracks in a thin air-filled hollow cylinder by application of the DORT method to elastic components of the echo," *Ultrasonics*, Vol. 40, 715–720, 2002.
7. Mordant, N., C. Prada, and M. Fink, "Highly resolved detection and selective focusing in a waveguide using the D. O. R. T. method," *The Journal of the Acoustical Society of America*, Vol. 105, 2634–2642, 1999.
8. Tortel, H., G. Micolau, and M. Saillard, "Decomposition of the time reversal operator for electromagnetic scattering," *Journal of Electromagnetic Waves and Applications*, Vol. 13, No. 5, 687–719, 1999.
9. Prada, C., S. Manneville, D. Spoliansky, and M. Fink, "Decomposition of the time reversal operator: Detection and selective focusing on two scatterers," *The Journal of the Acoustical Society of America*, Vol. 99, 2067–2076, 1996.
10. Prada, C. and J.-L. Thomas, "Experimental subwavelength localization of scatterers by decomposition of the time reversal operator interpreted as a covariance matrix," *The Journal of the Acoustical Society of America*, Vol. 114, 235–243, 2003.
11. Devaney, A. J., "Super-resolution processing of multi-static data using time reversal and MUSIC," http://www.ece.neu.edu/faculty/devaney/preprints/paper02n_00.pdf.
12. Lehman, S. K. and A. J. Devaney, "Transmission mode time-

- reversal super-resolution imaging,” *The Journal of the Acoustical Society of America*, Vol. 113, 2742–2753, 2003.
13. Miwa, T. and I. Arai, “Super-resolution imaging for point reflectors near transmitting and receiving array,” *IEEE Transactions on Antennas and Propagation*, Vol. 52, 220–229, 2004.
 14. Baussard, A. and T. Boutin, “Time-reversal RAP-MUSIC imaging,” *Waves in Random and Complex Media*, Vol. 18, 151–160, 2008.
 15. Simonetti, F., “Multiple scattering: The key to unravel the subwavelength world from the far-field pattern of a scattered wave,” *Physical Review E (Statistical, Nonlinear, and Soft Matter Physics)*, Vol. 73, 036619-13, 2006.
 16. Simonetti, F., “Pushing the boundaries of ultrasound imaging to unravel the subwavelength world,” *Proceedings of IEEE International Ultrasonics Symposium, Vancouver, Canada*, 313–316, 2006.
 17. Simonetti, F., M. Fleming, and E. A. Marengo, “Illustration of the role of multiple scattering in subwavelength imaging from far-field measurements,” *J. Opt. Soc. Am. A*, Vol. 25, 292–303, 2008.
 18. De Rosny, J. and C. Prada, “Multiple scattering: The key to unravel the subwavelength world from the far-field pattern of a scattered wave,” *Physical Review E (Statistical, Nonlinear, and Soft Matter Physics)*, Vol. 75, 048601-2, 2007.
 19. Minonzio, J.-G., C. Prada, A. Aubry, and M. Fink, “Multiple scattering between two elastic cylinders and invariants of the time-reversal operator: Theory and experiment,” *The Journal of the Acoustical Society of America*, Vol. 120, 875–883, 2006.
 20. Moura, J. M. F. and J. Yuanwei, “Detection by time reversal: Single antenna,” *IEEE Transactions on Signal Processing*, Vol. 55, 187–201, 2007.
 21. Moura, J. M. F. and J. Yuanwei, “Time reversal imaging by adaptive interference canceling,” *IEEE Transactions on Signal Processing*, Vol. 56, 233–247, 2008.
 22. Minonzio, J.-G., M. Davy, J. de Rosny, C. Prada, and M. Fink, “Theory of the time-reversal operator for the dielectric cylinder using separate transmit and received arrays,” *IEEE Transactions on Antennas and Propagation*, August 2009.
 23. Stewart, G. W., “Perturbation theory for the singular value decomposition,” *SVD and Signal Processing, II: Algorithms, Analysis and Applications*, 99–109, 1990.
 24. Xu, Z., “Perturbation analysis for subspace decomposition with

- applications in subspace-based algorithms,” *IEEE Transactions on Signal Processing*, Vol. 50, 2820–2830, 2002.
25. Zhenhua, L., “Direct perturbation method for reanalysis of matrix singular value decomposition,” *Applied Mathematics and Mechanics*, Vol. 18, 471–477, 1997.
 26. Liu, J., X. Liu, and X. Ma, “First-order perturbation analysis of singular vectors in singular value decomposition,” *IEEE Transactions on Signal Processing*, Vol. 56, 3044–3049, 2008.
 27. De Moor, B., “The singular value decomposition and long and short spaces of noisy matrices,” *IEEE Transactions on Signal Processing*, Vol. 41, 2826–2838, 1993.